THE JOURNAL OF PHYSICAL CHEMISTRY B

Article

pubs.acs.org/JPCB

An Insight into the Regiospecificity of Linoleic Acid Peroxidation Catalyzed by Mammalian 15-Lipoxygenases

Reynier Suardíaz,[†,‡] Laura Masgrau,[‡] José M. Lluch,[†,‡] and Àngels González-Lafont*[,†,‡]

[†]Departament de Química and [‡]Institut de Biotecnologia i de Biomedicina (IBB), Universitat Autònoma de Barcelona, 08193 Bellaterra, Barcelona, Spain

Supporting Information

ABSTRACT: 15-Lipoxygenases (15-LOs) catalyze the peroxidation reaction of linoleic acid (LA) in mammals producing almost exclusively 13-(*S*)-hydroperoxyoctadecadienoic acid (13-(*S*)-HPODE). Although several hypotheses have been formulated, the molecular basis of such enzymatic regiospecificity is unclear. We have here combined quantum mechanics/molecular mechanics (QM/MM) calculations with molecular dynamics simulations to analyze the peroxidation mechanism using a complete rabbit 15-LO-1/LA solvated model. C_9 and C_{13} being equivalent for planarity and spin density, the QM/MM potential energy profiles of the O_2 addition to those two atoms were calculated. The difference in the potential energy barrier heights is clear enough to justify that O_2 selectively attacks C_{13} giving 13-(*S*)-HPODE. Oxygenation at C_9 is hindered by two steric-shielding residues (Leu597 and Gln548). The calculated free energy profile at 300 K for the O_2 addition to C_{13} confirms that the peroxidation on C_{13} is a reversible viable process in agreement with experiments. Thus, the subsequent reduction of the peroxyl radical to give the final hydroperoxidated product is expected to give the irreversibility character to the overall process.

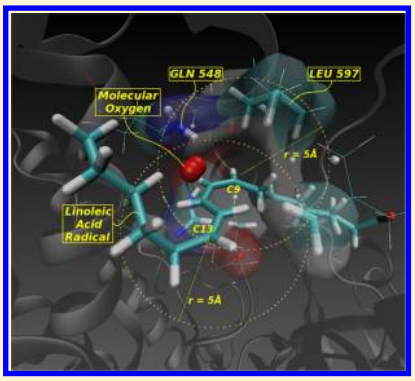

1. INTRODUCTION

15-Lipoxygenases (15-LOs) are lipid peroxidizing enzymes that catalyze the regio- and stereoselective introduction of molecular dioxygen to free and/or esterified polyunsaturated fatty acids (PUFAs) containing at least one 1,4-*Z*,*Z*-pentadiene group.[1,2] Among 15-LOs, 15-LO-1 is the key enzyme for lipid oxidation in macrophages, both in animal models and in humans, by catalyzing the oxidation of linoleic acid (LA; C18:2, omega-6) by O_2.[3] LA is the most abundant (40−45%) fatty acid in atherosclerotic plaques, being 7 times more abundant than arachidonic acid (AA), and it has been reported that 30% of PUFAs in plaques are oxidized.[3] The oxidized derivatives of LA, 9- and 13-hydroxyoctadecadienoic acid (9-HODE and 13-HODE), are also abundant in atherosclerotic lesions and regulate cellular pathways. However, in mammals reaction of LA with 15-LO-1 produces almost exclusively 13-(*S*)-HODE at the early stages of atherosclerosis disease, with 13-(*S*)-HODE actions being protective.[4,5] In contrast, the nonenzymatic oxidation of LA that occurs in later disease produces an approximately equal mixture of 9-(*R*)-HODE, 9-(*S*)-HODE, 13-(*R*)-HODE, and 13-(*S*)-HODE. In this case, pro-inflammatory actions of 9-HODE have been described that contribute to lesion progression.[3] Whether produced enzymatically or nonenzymatically, the synthesis of 13-HODE and 9-HODE takes place by fast reduction from their corresponding unstable hydroperoxy counterparts, 13-hydroperoxyoctadecadienoic acid (13-HPODE) and 9-hydroperoxyoctadecadienoic acid (9-HPODE), respectively.

Mechanistically, the overall hydroperoxidation process leading to those hydroperoxy products in LOs has been proposed to proceed through three main chemical reactions:[1] (1) stereoselective hydrogen abstraction from a substrate bisallylic carbon atom by the Fe(III)−OH^- cofactor, forming a carbon-centered substrate radical and Fe(II)−OH_2; (2) Substrate radical rearrangement and regio-stereospecific insertion of an oxygen molecule forming an oxygen-centered peroxy radical; and (3) reduction of the peroxy radical by hydrogen transfer from the Fe(II)−OH_2 moiety to give the final hydroperoxy product. However, in contrast to the diverse regio- and sterochemical outcomes of solution phase PUFAs autoxidation, LOs exert exquisite reaction specificity.[6] As a matter of fact, the explanation of the regiospecificity of the lipoxygenases at the molecular level has been an intriguing major goal of research for years. In 15-LO-1, only the C_{11} pro-S H-atom of LA is abstracted, followed by oxygen attack at C_{13} on the opposite face of the substrate (antarafacial relationship between H-removal and oxygenation), to give the 13-(*S*)-hydroperoxy radical that, after reduction, finally leads to 13-(*S*)-HPODE. In 15-LO-1 dual specificity has been observed with arachidonic fatty acid (AA) as substrate, although rabbit 15-LO-1 (15-rLO) shows a higher regiospecificity (ratio of 90:10[7,8] and 97:3[9] for human and rabbit enzymes, respectively) for C_{13} pro-S H-atom abstraction followed by oxygen attack at C_{15}

Received: December 26, 2012
Revised: March 11, 2013
Published: March 15, 2013

dx.doi.org/10.1021/jp312747q | *J. Phys. Chem. B* 2013, 117, 3747−3754

versus C_{10} pro-S H-atom abstraction followed by oxygen attack at C_{12}. On the other hand, it appears that the dominant H(P)ODEs formed in vivo have Z,E diene geometry, the Z,E/E,E HODE product ratio being about 6 in human plasma and close to 20 for mouse liver.[10]

From the structural point of view, the revised crystal structure of the mammalian 15-rLO with and without an inhibitor bound (PDB entry code 2P0M)[11] is available, showing an important conformational change of the enzyme upon ligand binding. This conformational transition mainly affects the α2-, α3-, and α18-helixes. In addition, early mutagenesis studies revealed the importance of Phe353, Ile418, Met419, Ile593, and Arg403 (15-rLO numbering) in regiospecificity.[9,12] Then, the triad concept was first developed as a simple explanation of rabbit 12/15-LOs[9] reaction specificity, suggesting that polyenoic fatty acids enter the substrate-binding pocket in the "tail-first" way (methyl end first) with the carboxylate remaining outside to interact with Arg403. According to the triad hypothesis, the alterations in the side-chain geometry of three residues, Phe353, Ile418, and I593, which are lining the bottom of the substrate-binding pocket, modify the volume of the active site. If the triad positions are occupied by small residues, fatty acid substrates are capable of penetrating deeper into the substrate-binding pocket so that hydrogen abstraction from C_{10} (oxygenation at C_{12}) is favored for AA, for example. In contrast, if more space-filling residues are located at these positions, hydrogen is mainly abstracted from C_{13} and oxygenation at C_{15} mainly takes place for AA. An important number of site-directed mutagenesis studies[13,14] on different 12/15-LOs have supported this concept but now it has been proven that it does not constitute a comprehensive model explaining the reaction specificity of all animal LO-isoforms.[13,15] Thus, it has also been proposed that different substrates could bind in opposite orientations (methyl end or carboxylate end first) to control the site of oxygenation.[12]

The knowledge of how different substrates accommodate in the active sites of LOs is vital for the understanding of positional specificity in these enzymes. In two previous studies, LA and/or AA were successfully docked in the inhibitor-bound monomer of an homology model of 15-hLO-1.[16,17] The modes of binding obtained for both substrates were said to be consistent with mutagenesis experiments,[16] and some relevant interactions were highlighted also in comparison with experimental proposals.[17] Beyond this data, however, there was no direct molecular structural evidence on catalytically productive LO−fatty acid complexes. With this aim, we recently presented[18,19] two theoretical studies of AA and LA binding to 15-rLO. Quantum mechanical gas-phase calculations, protein−ligand docking, MD simulations, and in silico mutagenesis were carried out to study the binding modes of AA and LA at the molecular level. Our results showed that the unligated monomer of the heterodimer contained in the crystal structure of 15-rLO is not suited to accommodate any of its physiological substrates, LA and AA. On the contrary, the inhibitor-bound monomer of the crystal structure, which includes a significant conformational change of the α2-helix, seems to be a more reliable structural model for hosting the substrate in the active site. However, the Arg403 region (near the surface of the enzyme) in that crystal structure is not ready for binding either LA or AA yet, and 15-rLO, which is flexible enough, adapts to the substrate by means of a reorganization of the hydrogen bond network in that region and sometimes by the displacement of the α2-helix. Relocation of Leu597 upon substrate binding, as seen in the crystal for inhibitor binding, is also confirmed by our molecular simulations. Very interestingly, AA and LA share a similar overall binding mode to 15-rLO. The carboxylate head of the fatty acids interact with Arg403, whereas the methyl ends lie in the nearby of Ile418 and Met419, as has been inferred from experimental mutagenesis data. The methyl end shows some more flexibility, especially for LA, which also presents smaller fluctuations at the reaction center. In contrast, sufficient space is available at the active site to allow conformational variability of AA, in particular for alternative positioning of the double bond system. This way, our results supported the sometimes referred as "boot-shaped" cavity for the 15-rLO:AA/LA complex as a plausible AA/LA binding mode ready for catalysis. It is worth noting that only some of those binding solutions were suitable for catalysis, that is, precatalytic complexes with short enough $C_{13}\cdots OH^-$ and/or $C_{10}\cdots OH^-$ distances (for AA) and $C_{11}\cdots OH^-$ distance (for LA) to initiate the H-abstraction process.

Because of the antarafacial character, hydrogen abstraction and oxygen insertion are mechanistically coupled but the structural basis for this coupling is unknown. It is also still unclear why certain LOs catalyze the carbon-centered C_n radical rearrangement (C_{11} in linoleic acid) in the direction of the CH_3 group ($[n + 2]$ rearrangement), and others in the direction of the COOH group ($[n - 2]$ rearrangement). Several hypotheses, related to electronic and steric effects, have been proposed:[1,2] (1) According to the *distortion hypothesis*, the otherwise planar pentadienyl radical moiety, in which the electronic density is equally distributed over the entire pentadienyl unit, experiments an enzyme-induced distortion that localizes the unpaired electron giving way to selective reaction with O_2 at that position. (2) According to the *delocalizing hypothesis* electron-withdrawing amino acids would be responsible for localizing the spin density of the fatty acid radical to a certain carbon atom of the pentadienyl unit. (3) According to the *oxygen targeting hypothesis*, oxygen is selectively targeted to a certain carbon atom, regardless of the electron density being equally distributed or not, so that only a particular peroxyl radical is formed; this can occur by means of a channel through the protein that may direct molecular oxygen to the desired site of oxygenation, or by means of steric-shielding residues at the active site that might block all but the desired center of the pentadienyl radical. (4) According to the *reduction hypothesis*, although oxygen can react with the fatty acid at many positions, all these reactions are reversible and formation of a distinct product depends on preventing further on−off reactions by selective reduction of the intended peroxyl radical. In the work by Klinman and co-workers[20] for soybean lipoxygenase-1 with LA as substrate, the oxygen targeting hypothesis via steric-shielding residues at the active site (Leu546 and Leu754 in that case) was confirmed with experiments using single-point mutants of the enzyme. The regio- and stereochemical aspects of the enzymatic PUFAs oxygenation have also been analyzed with experiments based on the observation that (*S*)-LOs have a conserved Ala at a critical position that is a Gly in (*R*)-LOs.[15,21−24] Coffa and Brash[21] showed that a single conserved active site residue directs oxygenation of AA stereospecificity in some lipoxygenases by carrying out mutation of the conserved Ala to Gly in mouse 8-(*S*)-LO and human 15-(*S*)-LO-2, and the corresponding Gly-Ala substitution in human 12-(*R*)-LO and coral 8-(*R*)-LO. However, Kühn and co-workers[24] have

recently shown that for mouse 5-(*S*)-LO and 12/15-(*S*)-LO from rabbits, men, rhesus monkeys, orangutans, and mice, only minor alterations in the reaction specificity were observed when the Ala-to-Gly exchange was performed. Molecular dynamics simulations by Furse et al.[25] verified the oxygen targeting hypothesis for cycloxygenase-1 and −2 with AA as substrate, and showed that one specific channel was involved in directing molecular oxygen to the active site where several residues were sterically shielding the undesirable sites of addition. In any case, and in order to correctly explain the experimentally determined product distribution, Furse et al. propose that the reduction hypothesis might also come into play.[25]

Our purpose with the present study is to analyze the molecular origin of the regiospecificity in the peroxidation of LA catalyzed by rabbit 15-LO-1 (15-rLO), the unique mammalian 15-LO enzyme with a resolved crystallographic structure. The major issue of how specific oxygenation is achieved by the enzyme, oxygen addition at C_{13} but not at C_9, will be analyzed. In trying to understand how the enzyme selects only a single outcome, some of the above-mentioned hypotheses will be considered.

2. THEORETICAL METHODS

In this paper, we have combined quantum mechanics/molecular mechanics (QM/MM) calculations with molecular dynamics (MD) simulations. Starting geometries have been taken from a previous work[19] where most likely complexes of 15-rLO with LA were obtained as follows. In brief, the coordinates of the enzyme were taken from the inhibitor-bound conformer of the PDB code 2P0M; the inhibitor was deleted and the hydroxide anion was modeled. Protein−ligand docking calculations were then carried out to bind LA into the active site of the enzyme; the best docking solution consistent with catalysis and experimental mutagenesis data was selected, fully solvated and equilibrated by performing molecular dynamics simulations in periodic boundary conditions. The structures used in this work were taken from these simulations, but a solvation sphere of 15 Å was kept. Notice that the inhibitor-bound form was preferred over the unligated conformer (also present in the PDB) as docking calculations to both conformers indicated that binding of LA to the unligated form in a catalytically competent binding mode, and in agreement with experimental mutagenesis data, was not feasible. All the QM/MM calculations have been carried out with the modular package Chemshell[26] using TURBOMOLE[27] for all the DFT calculations, and MNDO99[28] for the semiempirical ones. The MM part was treated in all cases with CHARMM22[29,30] and CHARMM27[31,32] (for the moiety of LA included in the MM region) force field through DL_POLY[33] module in Chemshell. Ad hoc parameters for the simulation of the Fe(II) coordination system have been used. An electronic embedding scheme[34] has been adopted in all the calculations and hydrogen link atoms have been used to treat the QM/MM boundary with the charge shift model.[35] No cutoffs were introduced for the nonbonding MM and QM/MM interactions. QM/MM optimizations were carried out using the low-memory Broyden−Fletcher−Goldfard−Shanno (L-BFGS)[36,37] algorithm in the case of minimizations and the microiterative optimizer combining both the partitioned rational function optimizer (P-RFO)[38,39] and L-BFGS[36,37] during the transition-state search. All these algorithms are implemented in the HDLCopt[40] module of Chemshell. In the two sets of QM/MM-MD simulations the system was gradually heated from 20 to 300 K in 1.5 ps and equilibrated at 300 K for 5 ps. The bonds involving hydrogen atoms in the MM region were fixed by the SHAKE algorithm. The free energy profile for the peroxidation reaction was obtained by means of the free energy perturbation method, freezing the electronic density of the QM part during the dynamics at frozen QM geometry, and approximating that density by electrostatic-potential-fitted point charges.[41] The spin density was evaluated as the difference between the α and the β NPA[42] (natural population analysis) net atomic charges, that is, as the α-spin excess.

3. RESULTS AND DISCUSSION

First, the distortion and the delocalization hypotheses have been studied. As mentioned before, the distortion hypothesis

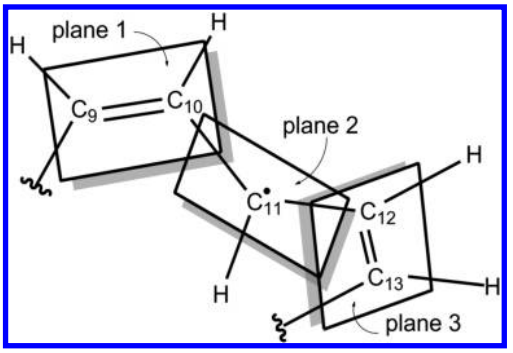

Figure 1. Three planes that should be nearly coincident due to the conjugation of the unpaired electron at C_{11} and the 4 π-electrons of the adjacent double bonds. The depicted configuration represents a possible geometry just after the H-abstraction and rehybridization of C_{11}.

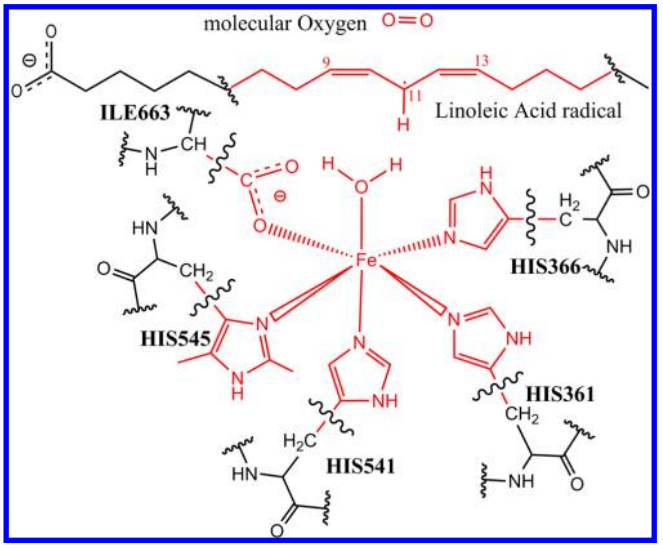

Figure 2. QM atoms are depicted in red. The boundary between QM and MM regions is indicated by wavy lines. This scheme represents the products of the first-step of the reaction mechanism and the reactants of the second step.

establishes that preferential localization of the spin density on a certain carbon atom can be favored by distortion of planarity of the LA-pentadienyl radical moiety. Once H_{11} of LA has been abstracted (first step of the reaction mechanism), the product radical is left in a very unstable geometry. Immediately, C_{11} approximately acquires an sp^2 hybridization (according to

dx.doi.org/10.1021/jp312747q | J. Phys. Chem. B 2013, 117, 3747−3754

Table 1. Dihedral Angles (in deg) Determining the Planarity of LA Radical ($C_9C_{10}C_{11}C_{12}$ and $C_{10}C_{11}C_{12}C_{13}$) before and after Geometry Optimization of Structures Taken from Ref 19

dihedral $C_9C_{10}C_{11}C_{12}$		dihedral $C_{10}C_{11}C_{12}C_{13}$	
before geometry optimization	after geometry optimization	before geometry optimization	after geometry optimization
288	347	265	179
293	185	280	189
245	182	126.2	179
256	193	128	182
99	14	130	180

natural bond orbital analysis)[43−45] and the radical moiety tends to planarity by conjugation in a π system consisting of 5 electrons (the unpaired electron originally at C_{11} and 4 π electrons of the adjacent double bonds) delocalized over 5 carbon atoms (from C_9 to C_{13}). There are three planes just after the H-abstraction that should be nearly coincident in order to reach full conjugation: the plane containing the double bond C_9═C_{10}, the plane involving the rehybridized C_{11}, and the plane containing the C_{12}═C_{13} double bond (see Figure 1). The value of the dihedral angle C_9−C_{10}−C_{11}−C_{12} must be close to 0° or 180° to ensure that the planes 1 and 2 are coincident and that the unpaired electron at C_{11} can delocalize up to C_9. The same applies to the dihedral angle C_{10}−C_{11}−C_{12}−C_{13}, the planes 2 and 3, and the unpaired electron delocalization up to C_{13}. Bulky effects of amino acid side chains

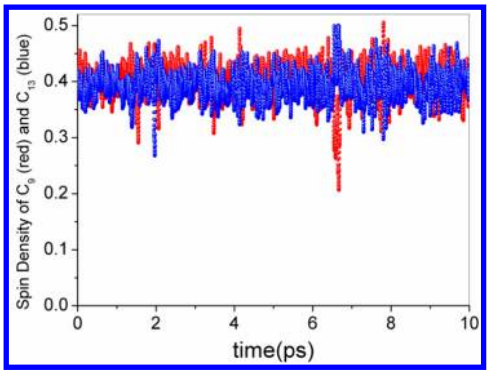

Figure 4. Spin densities on C_9 (red) and C_{13} (blue) along the QM(B3LYP)/MM-MD trajectory.

present in the active site could encumber the radical to adopt its fully planar form as outside the enzyme. In such a case, one of the mentioned dihedral angles could be much closer to the planarity than the other one, thereby promoting the oxygen addition to the corresponding carbon atom (the one with a greater spin density).

We have combined QM/MM calculations with MD simulations to analyze that possible effect of 15-rLO over the planarity of the LA-pentadienyl radical moiety (distortion hypothesis). Five precatalytic structures (i.e., with one of the H_{11} of LA close to the hydroxyl oxygen of the Fe(III)−OH^- cofactor and pointing to it) of 15-rLO:LA complexes have been selected from a previous work in which the most probable

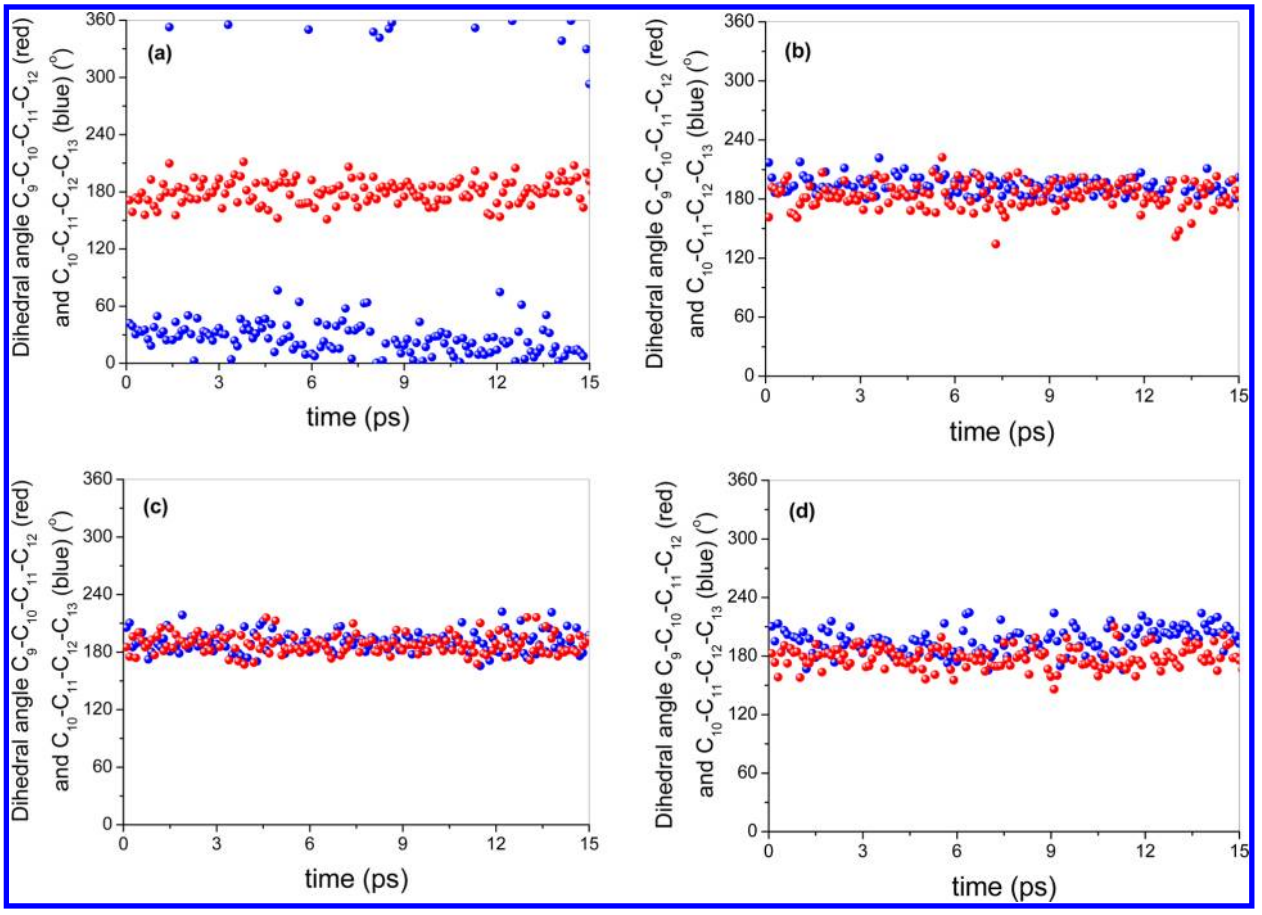

Figure 3. Analysis of dihedral angles along the QM/MM-MD trajectories for the first four optimized geometries of 15-rLO:LA complex.

dx.doi.org/10.1021/jp312747q | J. Phys. Chem. B 2013, 117, 3747−3754

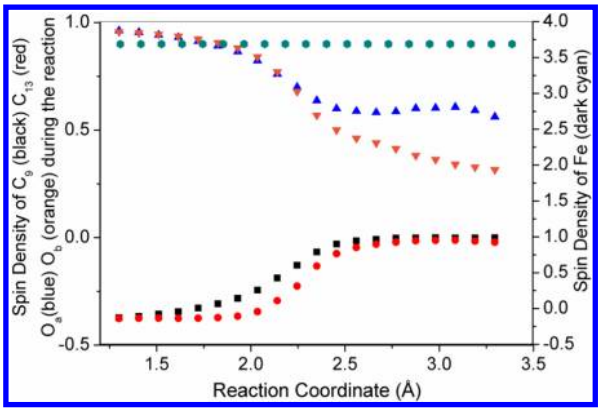

Figure 5. Spin densities on atoms C_9, C_{13}, O_a, O_b, and Fe during the reaction.

positions of LA within mammalian 15-rLO were determined.[18,19] They were also chosen to be far from planar (the two dihedral angles indicated in Figure 1 quite close to 90°). The corresponding geometries were manually modified in order to obtain a first distorted LA-pentadienyl radical corresponding to the product of the H-abstraction step of the reaction mechanism. For this, the H_{11} of LA was trimmed and bonded to the oxygen of the Fe(III)−OH^- cofactor at typical values of water bond distance and angle. Next, the substrate and all protein residues and water molecules within 15 Å of the C_{13} of LA (2189 atoms) were fully optimized at the QM(B3LYP)/MM level in conjunction with the 6-31G(d) basis set, except for Fe for which LANL2DZ was employed. The QM region (red atoms in Figure 2 but the molecular oxygen) consisted of 67 atoms (link atoms not included). The values of the dihedral angles C_9−C_{10}−C_{11}−C_{12} and C_{10}−C_{11}−C_{12}−C_{13} are shown in Table 1 before and after the geometry optimization. The results indicate that the conditions within the enzyme permit that the LA-pentadienyl-radical moiety reaches practically its totally planar form even starting from a considerably distorted geometry.

In addition, to locate the minimum-energy structures, the effect of thermal fluctuations on the planarity of the radical was also tested. For that purpose, four of those 15-rLO:LA optimized structures were used as starting coordinates for different QM(OM3)/MM-MD[46] simulations of 15 ps production run each. In this case, the QM region was defined as the red part of LA in Figure 2 (from C_6 to C_{17}). Figure 3 shows the variation of the dihedral angles C_9−C_{10}−C_{11}−C_{12} and C_{10}−C_{11}−C_{12}−C_{13} along the simulations. As it can be seen, most of the time the deviations from planarity reflected by those two dihedral angles are not important, with similar oscillating behavior for both of them, reinforcing the previous conclusion that the LA-pentadienyl-radical moiety is mostly planar within the enzyme.

Table 2. Distances (in Å) between the Oxygen Atom (O_b) Closer to the Carbon Atom to Which Is Added and the Closest Residues to C_9 and C_{13} at the Corresponding Pre-reactive Minima

addition to C_9				addition to C_{13}	
Gln548-Nε	2.82	Leu597-Cδ	3.10	Leu408-Cδ2	3.66
Gln548-Cδ	3.88	Leu597-Cβ	3.43	Leu408-Cδ1	3.99
Gln548-Oε	4.18	Leu597-Cγ	3.83	Leu408-Cγ	4.22

For the sake of completeness, we tried to discard any preferential localization of the unpaired electron on a favored carbon atom (delocalization hypothesis) by calculating the spin density (SD) on the fatty acid radical using a higher electronic structure level of calculation. To this aim, one of the five previously mentioned 15-rLO:LA optimized structures was used to run a QM(B3LYP/6-31G(d))/MM-MD 10 ps long simulation using the same QM part as in the previous QM/MM-MD simulations. The SDs at the C_9 and C_{13} carbon atoms were calculated and monitored during this MD trajectory. As it can be seen in Figure 4, both SDs fluctuate in an equivalent way around the same central value (roughly 0.4 au), suggesting that the regiospecificity of the peroxidation has no relation with any preferential localization of the unpaired electron on one of the two reactive carbon atoms.

At this point, C_9 and C_{13} being equivalent for planarity and spin density, the potential energy profiles of the O_2 addition to those two carbon atoms should be able to explain why the hydroperoxidation occurs almost exclusively on C_{13}. In a previous work, Saam et al.[47] computed the 3D free energy distribution for O_2 inside the substrate-free 15-rLO and identified four channels connecting the protein surface with a region of high oxygen affinity at the active site. This region is located deep inside the substrate-binding pocket opposite to the nonheme iron. When AA was added to the system, the regions of highest oxygen affinity at the active site were not altered significantly. Following that study and starting from one of the above-mentioned five 15-rLO:LA optimized structures, we have placed an oxygen molecule at several locations in the active site taking into account the high probability region described by Saam et al.,[47] which being at the opposite side of

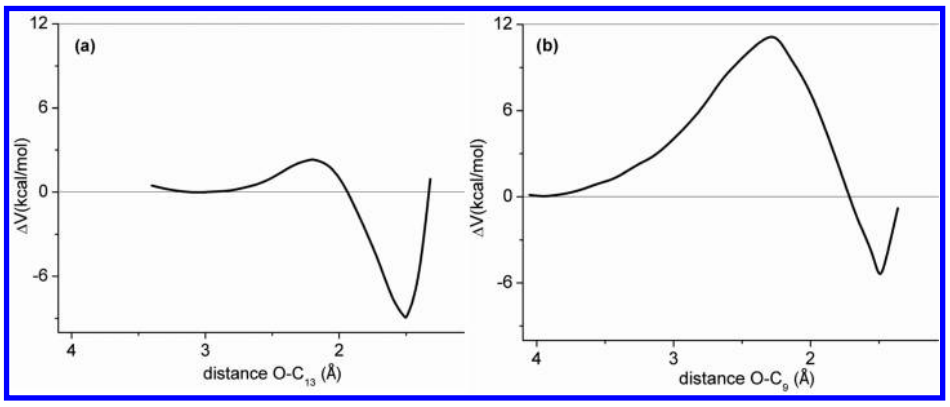

Figure 6. Potential energy profiles for O_2 addition on C_{13} (a) and C_9 (b).

dx.doi.org/10.1021/jp312747q | J. Phys. Chem. B 2013, 117, 3747−3754

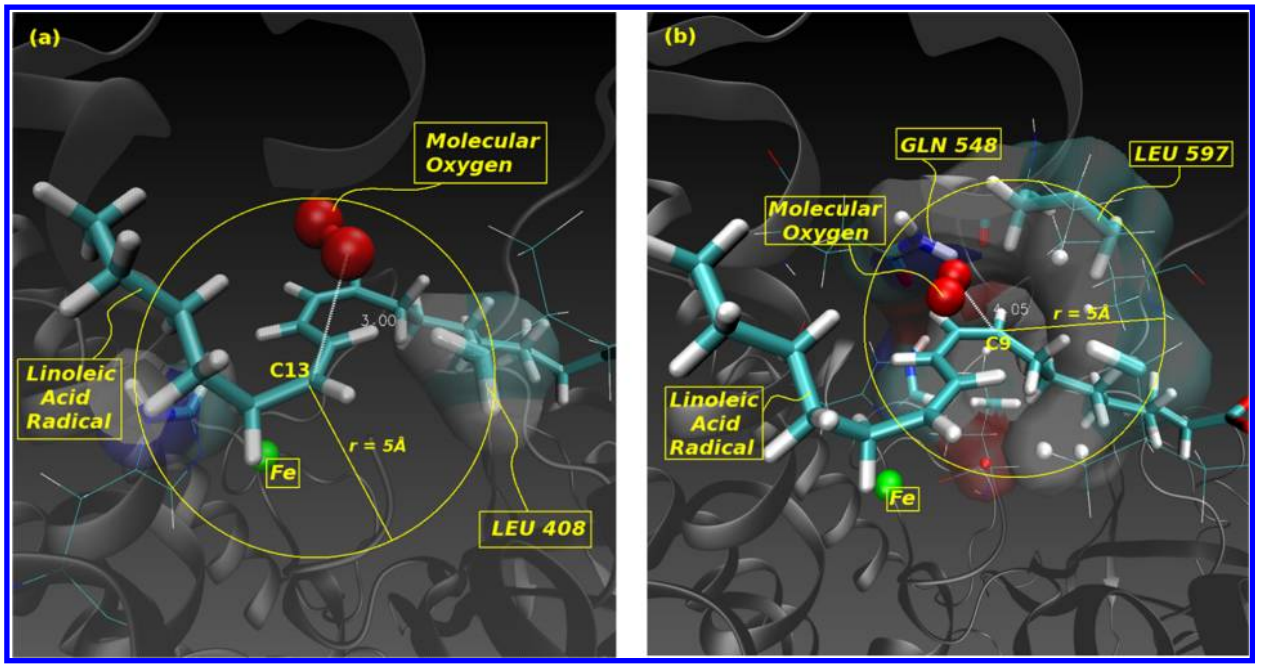

Figure 7. Relative positions of molecular oxygen and LA radical at the prereactive minima: (a) prereactive minimum for reaction at C_{13}; (b) prereactive minimum for reaction at C_9. Molecular oxygen and all the protein atoms within a sphere of 5 Å centered at carbon C_{13} (a) and at carbon C_9 (b) are highlighted by using licorice drawing method. Water molecules are not depicted.

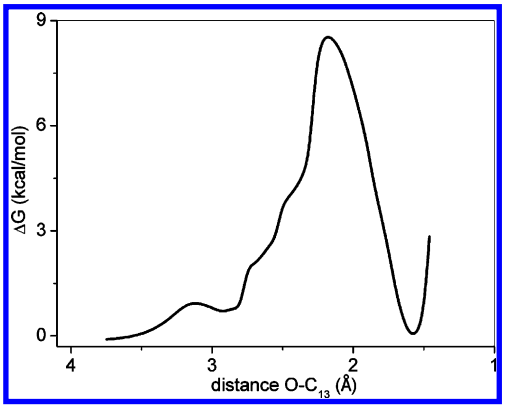

Figure 8. Free energy profile for O_2 addition on C_{13}.

Fe regarding LA is also consistent with the antarafacial nature of the H-abstraction and the O_2-addition step of the reaction mechanism. In fact, the LA radical arrangement in our simulations is such that the O_2 molecule can only approach the fatty acid radical from the opposite site of the iron atom. Thus, our molecular simulations are also in accordance with the antarafacial character of the oxygen addition in 15-rLO that determines the stereoselectivity of the LA peroxidation process giving only the 13-(*S*)-HPODE stereoisomer. Various geometry optimizations were carried out with O_2 close to the LA-pentadienyl radical until finding two prereactive minima. Those minima were used as starting points of the potential energy profiles for the addition of O_2 to the positions C_{13} and C_9 of the LA-pentadienyl radical. The reaction paths were scanned by performing constrained geometry optimizations along the reaction coordinate $O-C(C_{13}/C_9)$ by steps of 0.1 Å. The QM region for all those geometry optimizations (and for the free energy calculations, see below) includes now all the red atoms in Figure 2, and it is described at the B3LYP/6-31G(d) level, except for Fe for which the LANL2DZ basis set was used. In all, the system involves 12 892 atoms, 2191 being mobile.

As the current system can be troublesome in terms of the SDs, those spin densities were checked along the potential energy profiles on certain atoms as it is shown in Figure 5. The SDs on C_{13} and C_9 go from −0.4 au to 0 au each, and the SDs on each oxygen atom go from 1 au to 0.6 au or 0.4 au (the oxygen atom (O_b) closer to the carbon atom to which is being added) due to the formation of the peroxide bond. It is noteworthy that the SD on Fe(II) remains unchanged (3.7 au) along the O_2 addition. This suggests that Fe has no effect on the O_2 addition, as quoted previously by Knapp et al.[48]

The potential energy profiles for the O_2 addition to C_{13} and C_9 are shown in Figure 6. Those profiles provided starting structures for subsequent direct localization of the transition state structures. Frequency calculations on the QM region confirmed that all the located transition state structures are characterized by a single imaginary frequency and a suitable transition vector that corresponds to the investigated reaction. The transition-state structure for the O_2 addition to C_{13} involves an energy barrier as small as 2.33 kcal/mol, while the barrier height for the reaction on C_9 is significantly larger, 11.27 kcal/mol. The difference in the potential energy barrier heights is clear enough to justify that O_2 selectively attacks C_{13} and it can be understood taking a deeper look inside the cavity where the LA-pentadienyl radical is located. Once the O_2 is at the positions of the prereactive minima, it is quite difficult to reach C_9 due to the hindrance of the side chains of Leu597 and Gln548 (Figure 7b). Conversely, it is very easy to reach C_{13} (Figure 7a). Notice, moreover, that Leu408 lies in the plane of the pentadienyl radical whereas Leu597/Gln548 are situated over this plane, in the region where the π density is. Thus, Leu597 and Gln548 interfere with the trajectory for O_2 approximation to C_9 but Leu408 does not for C_{13} (see Figure 7). This statement can be confirmed at molecular level if we look at the intermolecular distances between the oxygen

dx.doi.org/10.1021/jp312747q | *J. Phys. Chem. B* 2013, 117, 3747−3754

molecule and the protein residues closest to the attacked carbon atom at each prereactive minimum. Thus, the distances between O_b (see Table 2) in Figure 7b and Leu597 and Gln548 are clearly shorter than the O_b···Leu408 distance in Figure 7a. It is also worth noting that the O_2 at the prereactant minimum of the addition on C_{13} (which resembles that in gas phase[49]) is located at only 3.0 Å to C_{13}, while at the prereactant minimum of the addition on C_9 is farther, at 4.0 Å to C_9. This is also because of the presence of nearby residue side chains. Indeed, a definitive test of our proposal about the functional relevance of residues Leu597 and Gln548 would be the study of the O_2 addition to suitable mutants of 15-rLO. Ongoing work in this direction is being done now in our laboratory using the in silico approach, and we expect that in vitro site-directed mutagenesis studies might be also carried out by experimental groups in a near future.

Once discarded the addition to C_9, we have used the free-energy perturbation method to determine the free energy profile at 300 K for the O_2 addition to C_{13} (see Figure 8). The increasing relevance of the entropic effects as O_2 approaches C_{13} clearly increases the barrier (the free energy barrier becomes 8.68 kcal/mol) and converts a quite exergonic addition (see Figures 6a and 8) in a process with a roughly null reaction free energy. These results show that the O_2 addition and dissociation turn out to proceed with a similar rate constant, the peroxidation on C_{13} being a reversible process in agreement with experiments corresponding to O_2 addition to carbon radicals.[6] As a matter of fact, it is the reduction of the peroxyl radical to form 13-(*S*)-HPODE that makes the global hydroperoxidation process irreversible.

4. CONCLUSIONS

In this paper, the first theoretical study of the molecular mechanism of the linoleic acid (LA) peroxidation catalyzed by rabbit 15-LO-1 (15-rLO) is given by means of quantum mechanics/molecular mechanics (QM/MM) calculations and molecular dynamics (MD) simulations on a complete 15-rLO:LA solvated model. We have shown that the high regiospecificity of the LA peroxidation (at C_{13} but not at C_9) catalyzed by this enzyme can be explained by the oxygen targeting hypothesis via steric-shielding residues (particularly Leu597 and Gln548) at the active site of the enzyme. This can be the reason why, with LA as substrate, the enzyme 15-LO-1 in mammals produces almost exclusively 13-(*S*)-HODE at the early stages of atherosclerosis disease. We expect that the new physical insights reported here can stimulate new experiments and might contribute to the development of new atheroprotective agents.

■ ASSOCIATED CONTENT

Supporting Information

Complete refs 26 and 30. This material is available free of charge via the Internet at http://pubs.acs.org.

■ AUTHOR INFORMATION

Corresponding Author

*E-mail: Angels.Gonzalez@uab.cat. Tel.: (+34) 935811672.

Notes

The authors declare no competing financial interest.

■ ACKNOWLEDGMENTS

We thank the Spanish Ministerio de Economía y Competitividad (Grant CTQ2011-24292) and the Generalitat de Catalunya (2009SGR409) for financial support. L.M. thanks the "Ramon y Cajal" program. R.S. acknowledges the Alianza 4U program. We also acknowledge CESCA for computational facilities.

■ REFERENCES

(1) Ivanov, I.; Heydeck, D.; Hofheinz, K.; Roffeis, J.; O'Donnell, V. B.; Kühn, H.; Walther, M. *Arch. Biochem. Biophys.* **2010**, *503*, 161.
(2) Schneider, C.; Pratt, D. A.; Porter, N. A.; Brash, A. R. *Chem. Biol.* **2007**, *14*, 473.
(3) Vangaveti, V.; Baune, B. T.; Kennedy, R. L. *Ther. Adv. Endocrinol. Metab.* **2010**, *1*, 51.
(4) Kühn, H.; Belkner, J.; Zaiss, S.; Fahrenklemper, T.; Wohlfeil, S. *J. Exp. Med.* **1994**, *179*, 1903.
(5) Jostarndt, K.; Gellert, N.; Rubic, T.; Weber, C.; Kühn, H.; Johansen, B.; Hrboticky, N.; Neuzil, J. *Biochem. Biophys. Res. Commun.* **2002**, *290*, 988.
(6) Yin, H. Y.; Xu, L. B.; Porter, N. A. *Chem. Rev.* **2011**, *111*, 5944.
(7) Jacquot, C.; Wecksler, A. T.; McGinley, C. M.; Segraves, E. N.; Holman, T. R.; van der Donk, W. A. *Biochemistry* **2008**, *47*, 7295.
(8) Gan, Q.-F.; Browner, M. F.; Sloane, D. L.; Sigal, E. *J. Biol. Chem.* **1996**, *271*, 25412.
(9) Borngraber, S.; Browner, M.; Gillmor, S.; Gerth, C.; Anton, M.; Fletterick, R.; Kühn, H. *J. Biol. Chem.* **1999**, *274*, 37345.
(10) Liu, W.; Yin, H. Y.; Akazawa, Y. O.; Yoshida, Y.; Niki, E.; Porter, N. A. *Chem. Res. Toxicol.* **2010**, *23*, 986.
(11) Choi, J.; Chon, J. K.; Kim, S.; Shin, W. *Proteins: Struct. Funct. Bioinf.* **2008**, *70*, 1023.
(12) Schwarz, K.; Borngraber, S.; Anton, M.; Kühn, H. *Biochemistry* **1998**, *37*, 15327.
(13) Vogel, R.; Jansen, C.; Roffeis, J.; Reddanna, P.; Forsell, P.; Claesson, H.-E.; Kühn, H.; Walther, M. *J. Biol. Chem.* **2010**, *285*, 5369.
(14) Bürger, F.; Krieg, P.; Marks, F.; Fürstenberger, G. *Biochem. J.* **2000**, *348*, 329.
(15) Meruvu, S.; Walther, M.; Ivanov, I.; Hammarstrom, S.; Furstenberger, G.; Krieg, P.; Reddanna, P.; Kühn, H. *J. Biol. Chem.* **2005**, *280*, 36633.
(16) Wecksler, A. T.; Kenyon, V.; Deschamps, J. D.; Holman, T. R. *Biochemistry* **2008**, *47*, 7364.
(17) Mascayano, C.; Núñez, G.; Acevedo, W.; Rezende, M. *J. Mol. Model.* **2010**, *16*, 1039.
(18) Toledo, L.; Masgrau, L.; Maréchal, J. D.; Lluch, J. M.; González-Lafont, À. *J. Phys. Chem. B* **2010**, *114*, 7037.
(19) Toledo, L.; Masgrau, L.; Lluch, J. M.; González-Lafont, À. *J. Comput. Aided Mol. Des.* **2011**, *25*, 825.
(20) Knapp, M. J.; Seebeck, F. P.; Klinman, J. P. *J. Am. Chem. Soc.* **2001**, *123*, 2931.
(21) Coffa, G.; Brash, A. R. *Proc. Natl. Acad. Sci. U.S.A.* **2004**, *101*, 15579.
(22) Coffa, G.; Imber, A. N.; Maguire, B. C.; Laxmikanthan, G.; Schneider, C.; Gaffney, B. J.; Brash, A. R. *J. Biol. Chem.* **2005**, *280*, 38756.
(23) Coffa, G.; Schneider, C.; Brash, A. R. *Biochem. Biophys. Res. Commun.* **2005**, *338*, 87.
(24) Jansen, C.; Hofheinz, K.; Vogel, R.; Roffeis, J.; Anton, M.; Reddanna, P.; Kühn, H.; Walther, M. *J. Biol. Chem.* **2011**, *286*, 37804.
(25) Furse, K. E.; Pratt, D. A.; Schneider, C.; Brash, A. R.; Porter, N. A.; Lybrand, T. P. *Biochemistry* **2006**, *45*, 3206.
(26) Sherwood, P.; de Vries, A. H.; Guest, M. F.; Schreckenbach, G.; Catlow, C. R. A.; French, S. A.; Sokol, A. A.; Bromley, S. T.; Thiel, W.; Turner, A. J.; et al. *J. Mol. Struct. THEOCHEM* **2003**, *632*, 1.
(27) Ahlrichs, R.; Bär, M.; Häser, M.; Horn, H.; Kölmel, C. *Chem. Phys. Lett.* **1989**, *162*, 165.
(28) Thiel, W. *MNDO99 program, version 7.0*; Max-Planck-Institut für Kohlenforschung: Mülheim, Germany, 2005.

(29) MacKerell, A. D., Jr.; Feig, M.; Brooks, C. L. *J. Comput. Chem.* **2004**, *25*, 1400.
(30) MacKerell, A. D., Jr.; Bashford, D.; Bellott, M.; Dunbrack, R. L.; Evanseck, J. D.; Field, M. J.; Fischer, S.; Gao, J.; Guo, H.; Ha, S.; et al. *J. Phys. Chem. B* **1998**, *102*, 3586.
(31) Feller, S. E.; MacKerell, A. D., Jr. *J. Phys. Chem. B* **2000**, *104*, 7510.
(32) Feller, S. E.; Gawrisch, K.; MacKerell, A. D., Jr. *J. Am. Chem. Soc.* **2001**, *124*, 318.
(33) Smith, W.; Forester, T. R. *J. Mol. Graph.* **1996**, *14*, 136.
(34) Bakowies, D.; Thiel, W. *J. Phys. Chem.* **1996**, *100*, 10580.
(35) de Vries, A. H.; Sherwood, P.; Collins, S. J.; Rigby, A. M.; Rigutto, M.; Kramer, G. J. *J. Phys. Chem. B* **1999**, *103*, 6133.
(36) Nocedal, J. *Math. Comput.* **1980**, *35*, 773.
(37) Liu, D.; Nocedal, J. *Math. Program.* **1989**, *45*, 503.
(38) Banerjee, A.; Adams, N.; Simons, J.; Shepard, R. *J. Phys. Chem.* **1985**, *89*, 52.
(39) Baker, J. *J. Comput. Chem.* **1986**, *7*, 385.
(40) Billeter, S. R.; Turner, A. J.; Thiel, W. *Phys. Chem. Chem. Phys.* **2000**, *2*, 2177.
(41) Kästner, J.; Senn, H. M.; Thiel, S.; Otte, N.; Thiel, W. *J. Chem. Theory Comput.* **2006**, *2*, 452.
(42) Reed, A. E.; Weinstock, R. B.; Weinhold, F. *J. Chem. Phys.* **1985**, *83*, 735.
(43) Foster, J. P.; Weinhold, F. *J. Am. Chem. Soc.* **1980**, *102*, 7211.
(44) Glendening, E. D.; Landis, C. R.; Weinhold, F. *WIREs Comput. Mol. Sci.* **2012**, *2*, 1.
(45) Carpenter, J. E.; Weinhold, F. *J. Mol. Struct. THEOCHEM* **1988**, *169*, 41.
(46) Korth, M.; Thiel, W. *J. Chem. Theory Comput.* **2011**, *7*, 2929.
(47) Saam, J.; Ivanov, I.; Walther, M.; Holzhutter, H. G.; Kühn, H. *Proc. Natl. Acad. Sci. U.S.A.* **2007**, *104*, 13319.
(48) Knapp, M. J.; Klinman, J. P. *Biochemistry* **2003**, *42*, 11466.
(49) Tejero, I.; González-Lafont, À.; Lluch, J. M.; Eriksson, L. A. *J. Phys. Chem. B* **2007**, *111*, 5684.